HAL
open science

Chasing the observational signatures of seed black holes at z > 7: candidate observability

Rosa Valiante, Raffaella Schneider, Luca Zappacosta, Luca Graziani, Edwige Pezzulli, Marta Volonteri

To cite this version:

Rosa Valiante, Raffaella Schneider, Luca Zappacosta, Luca Graziani, Edwige Pezzulli, et al.. Chasing the observational signatures of seed black holes at z > 7: candidate observability. Monthly Notices of the Royal Astronomical Society, 2018, 476, pp.407-420. 10.1093/mnras/sty213 . insu-03747698

HAL Id: insu-03747698

https://insu.hal.science/insu-03747698v1

Submitted on 8 Aug 2022

HAL is a multi-disciplinary open access archive for the deposit and dissemination of scientific research documents, whether they are published or not. The documents may come from teaching and research institutions in France or abroad, or from public or private research centers.

L'archive ouverte pluridisciplinaire **HAL**, est destinée au dépôt et à la diffusion de documents scientifiques de niveau recherche, publiés ou non, émanant des établissements d'enseignement et de recherche français ou étrangers, des laboratoires publics ou privés.

Monthly Notices of the ROYAL ASTRONOMICAL SOCIETY

MNRAS **476,** 407–420 (2018)
Advance Access publication 2018 January 29

doi:10.1093/mnras/sty213

Chasing the observational signatures of seed black holes at $z > 7$: candidate observability

Rosa Valiante,[1★] Raffaella Schneider,[1,2] Luca Zappacosta,[1] Luca Graziani,[1] Edwige Pezzulli[1,2,3] and Marta Volonteri[4]

[1]*INAF-Osservatorio Astronomico di Roma, via di Frascati 33, I-00078 Monteporzio Catone, Italy*
[2]*Dipartimento di Fisica, Universitá di Roma 'La Sapienza', P.le Aldo Moro 2, I-00185 Roma, Italy*
[3]*INFN, Sezione di Roma I, P.le Aldo Moro 2, I-00185 Roma, Italy*
[4]*CNRS, UMR 7095, Institut d'Astrophysique de Paris, F-75014 Paris, France*

Accepted 2018 January 22. Received 2018 January 17; in original form 2017 September 20

ABSTRACT

Observing the light emitted by the first accreting black holes (BHs) would dramatically improve our understanding of the formation of quasars at $z > 6$, possibly unveiling the nature of their supermassive black hole (SMBH) seeds. In previous works, we explored the relative role of the two main competing BH seed formation channels, Population III remnants (low-mass seeds) and direct collapse BHs (high-mass seeds), investigating the properties of their host galaxies in a cosmological context. Building on this analysis, we predict here the spectral energy distribution and observational features of low- and high-mass BH seeds selected among the progenitors of a $z \sim 6$ SMBH. We derive the processed emission from both accreting BHs and stars by using the photoionization code CLOUDY, accounting for the evolution of metallicity and dust-to-gas mass ratio in the interstellar medium of the host galaxies, as predicted by the cosmological data-constrained model GAMETE/QSODUST. We show how future missions like *James Webb Space Telescope* (*JWST*) and *Advanced Telescope for High Energy Astrophysics* (ATHENA) will be able to detect the light coming from SMBH progenitors already at $z \sim 16$. We build upon previous complementary studies and propose a method based on the combined analysis of near-infrared colours, IR excess (IRX), and UV continuum slopes (i.e. colour–colour and IRX–β diagrams) to distinguish growing seed BH host galaxies from starburst-dominated systems in *JWST* surveys. Sources selected through this criterion would be the best target for follow-up X-ray observations.

Key words: galaxies: evolution – galaxies: high-redshift – galaxies: nuclei – quasars: general – quasar: supermassive black holes.

1 INTRODUCTION

Recent theories of black hole (BH) formation predict at least two viable mechanisms explaining the formation of accreting supermassive black holes (SMBHs) of 10^9–10^{10} $M_\odot$, which are observed already at redshift $z \sim 7$: the rapid growth of Population III (Pop III) remnant BHs ($\sim$100 $M_\odot$; e.g. Madau & Rees 2001; Heger et al. 2003; Yoshida, Omukai & Hernquist 2008; Latif et al. 2013; Hirano et al. 2015), driven by the accretion of gas at rates exceeding the Eddington limit or the formation of more massive BH seeds, the so-called direct collapse BHs (DCBHs), of (10^5–10^6) $M_\odot$ (e.g. Bromm & Loeb 2003; Begelman, Volonteri & Rees 2006; Lodato & Natarajan 2006, 2007; Volonteri, Lodato & Natarajan 2008; Inayoshi & Omukai 2012; Agarwal et al. 2014; Ferrara et al. 2014; Inayoshi, Visbal & Kashiyama 2015). We refer the readers to a number of dedicated reviews for more details on different seed formation and growth mechanisms (Volonteri 2010; Natarajan 2011; Johnson & Haardt 2016; Latif & Ferrara 2016; Gallerani et al. 2017; Valiante et al. 2017, and references therein).

Several semi-analytic models have been devoted to study the formation of SMBHs, exploring the role of low-mass or high-mass seeds (e.g. Volonteri, Haardt & Madau 2003; Haiman 2004; Madau et al. 2004; Volonteri & Rees 2005, 2006; Tanaka & Haiman 2009; Volonteri, Silk & Dubus 2015, and references therein). Petri, Ferrara & Salvaterra (2012) presented the first semi-analytic model for the formation of high-redshift SMBHs exploring the combined action of low- (100 $M_\odot$) and high-mass (10^5 $M_\odot$) seed BHs. In all those works, however, seeds were not planted according to the environmental conditions, and the chemical evolution of the interstellar medium (ISM) of the host galaxies was not considered.

In a previous work (Valiante et al. 2016, hereafter V16), we used a cosmological, data-constrained model GAMETE/QSODUST to investigate the relative role of low-mass (light) and high-mass (heavy)

★ E-mail: rosa.valiante@oa-roma.inaf.it

© 2018 The Author(s)
Published by Oxford University Press on behalf of the Royal Astronomical Society

Downloaded from https://academic.oup.com/mnras/article/476/1/407/4828380 by CNRS - ISTO user on 08 August 2022

BH seed in the formation of $z > 6$ SMBHs, like the one powering the quasar SDSS J1148+5251. GAMETE/QSODUST consistently follows the formation and evolution of nuclear BHs and their host galaxies along different merger histories of the parent dark matter (DM) halo. While many semi-analytical models and simulations follow BH growth, star formation, and metals, GAMETE/QSODUST is the only model that traces accurately dust evolution as well.

In V16, we showed that in a Eddington-limited BH accretion scenario, despite their low occurrence (in just few haloes, 3–30 depending on the merger history), the formation of DCBHs is required to grow a SMBH with $M_{\rm BH} > 10^9\,{\rm M}_\odot$. Moreover, in Pezzulli, Valiante & Schneider (2016), we showed that a mildly super-critical growth (less than 20 times the Eddington rate) on to light BH seeds of $100\,{\rm M}_\odot$ is required to reproduce the mass of SDSS J1148+5251 if heavy seeds are not considered in our model.

Despite intensive efforts, no observational signatures of high-redshift SMBH progenitors have been found in current surveys (see e.g. Reines & Comastri 2016, for a recent review). To date, no clear AGN signatures at $z > 6$ have been found even in the deepest X-ray observations (Willott 2011; Treister et al. 2013; Weigel et al. 2015; Cappelluti et al. 2016; Vito et al. 2016; Luo et al. 2017). It should be noted though that two faint AGN candidates, with photometric redshift $z = 6.6$ and 9.7, have been selected in the CANDELS GOODS-S field (Giallongo et al. 2015). Although the redshift determination is still uncertain (Georgakakis et al. 2015; Cappelluti et al. 2016; Luo et al. 2017), these sources have been proposed as possible DCBH hosts by Pacucci et al. (2016).

A clear example of the difficulties in interpreting observations at high redshift is the controversial nature of the metal-poor component of the bright Lyα emitter CR7 observed by Matthee et al. (2015), Sobral et al. (2015), and Bowler et al. (2017) at redshift $z \sim 6.6$. This is suggested to be either a DCBH (Hartwig et al. 2015; Pallottini et al. 2015; Agarwal et al. 2016, 2017; Smidt, Wiggins & Johnson 2016; Smith, Bromm & Loeb 2016; Pacucci et al. 2017) or a Pop III star host candidate (Sobral et al. 2015; Dijkstra, Gronke & Sobral 2016; Visbal, Haiman & Bryan 2016), or none of the two (Bowler et al. 2017).

If faint AGNs at high redshift are powered by accreting DCBHs, the non-detection of AGN candidates in current surveys may be explained by the peculiar and rare environmental conditions required for DCBH formation (Hosokawa, Omukai & Yorke 2012; Hosokawa et al. 2013; Dijkstra, Ferrara & Mesinger 2014; Inayoshi & Haiman 2014; Inayoshi, Omukai & Tasker 2014; Yue et al. 2014; Chon et al. 2016; Habouzit et al. 2016; Sugimura et al. 2016; V16). On the other hand, the current lack of detection in the X-ray band could be due to short and intermittent super-Eddington accretion events on Pop III remnants, resulting in a very low active BH fraction (~ 1 per cent) at $z > 7$ (Pezzulli et al. 2017).

Theoretical models of the expected spectral energy distribution (SED) of AGNs at $z > 4$–5 may provide a powerful tool to support future observations. Indeed, with the upcoming *James Webb Space Telescope* (*JWST*) and *Advanced Telescope for High Energy Astrophysics* (*ATHENA*, in the next decade) missions, we may be able to detect the signatures of active galaxies up to very high redshifts. Pacucci et al. (2015) modelled the SED of a growing DCBH with initial mass of $10^5\,{\rm M}_\odot$ accreting gas in a metal-free isolated DM host halo. They use the code CLOUDY (Ferland et al. 2013) to process the intrinsic (optical/UV/X-ray) emission, suggesting that the resulting infrared (IR) emission around $\sim 1\,\mu$m and the [0.1–10] keV band X-ray emission may be detected by *JWST* and *ATHENA*. Subsequently, Natarajan et al. (2017) extended this study to what they call *obese black hole galaxies* (OBGs), a class of transient objects predicted by Agarwal et al. (2013) that originate from the merging of star-forming galaxies with a neighbour satellite DCBH host. The authors presented a colour–colour selection criterion aimed at identifying OBGs with predicted magnitudes $M_{\rm AB} < 25$, which should be detected by the *JWST* instrument MIRI. They compared the SEDs of OBGs and of growing Pop III remnant BHs at redshift $z = 9$, concluding that *JWST* could be able to discriminate among the two seed formation channels. In addition, Volonteri et al. (2017) presented a population synthesis model for high-redshift BHs, AGN, and galaxies, based on empirical relations, proposing a colour–colour selection in *JWST* photometric bands, $F1280W - F2100W$ versus $F200W - F1280W$, to discriminate starburst-dominated galaxies and AGN in future surveys.

The studies mentioned above introduced promising methods to search for AGN and seed BH candidates in future surveys, setting the (theoretical) groundwork for the upcoming high-redshift multi-wavelength observations. However, the systems analysed in Natarajan et al. (2017) and Volonteri et al. (2017) are not explicitly related to the formation of a SMBH with the mass and accretion rate sufficient to explain the luminous quasars at $z \sim 6$ and do not grow in its environment.

In Valiante et al. (2018, hereafter Paper I), we presented a statistical analysis of the properties of 'isolated' galaxies that host light (low-mass) or heavy (high-mass) BH seeds.[1] We named these systems (BH + host galaxy) *isolated light seeds* (ILS) and *isolated heavy seeds* (IHS). Following V16, ILS and IHS have been selected among the progenitors of SDSS J1148+5251. In Paper I, we pointed out that at $z > 10$ the majority of heavy ($\sim$98 per cent) and light (80 per cent) seeds evolve in isolation and that these two populations show different properties: IHS have BH accretion rate (BHAR) higher than ILS; IHS host galaxies show a factor of 5–10 lower stellar mass and metallicity as well as a less efficient star formation history. These differences become statistically negligible at $z \leq 10$, when the fraction of IHS (ILS) drops to less than $\sim$2˜(20) per cent as a consequence of merger events. At these later epochs, any trace of the BH seed origin and of its birth environment is lost. Thus, candidate systems at $z > 10$ are the best targets to discriminate among the two main seed formation channels.

Here we compute the SED of IHS and ILS, using the sample presented in Paper I. Our aim is to establish the feasibility of (i) detecting high-z faint progenitors of the first SMBHs, (ii) observationally discriminating light and heavy BH seeds. Similarly to Pacucci et al. (2015) and Natarajan et al. (2017), we use CLOUDY to model the SEDs of IHS and ILS. The main difference of our approach is that we analyse systems (BHs–host galaxies) selected among the ancestor population of an observed SMBH, along its cosmological evolution. In other words, our approach has the advantage of following the evolution of light and heavy seed progenitors along the same hierarchical history (i.e. the two seed BH formation channels are not mutually exclusive), starting from the epoch at which the first stars form ($z \sim 24$), down to $z \sim 6$, when the observed quasar is eventually assembled. The properties of the seed BH population are closely related to the evolution of their host galaxies: mass, number, redshift distribution, and growth history are regulated by the build-up of the UV radiation field, by the metals and dust pollution of the ISM and intergalactic medium (IGM), and by the effect of stellar and AGN-driven winds. Our approach allows us to assess

[1] Starting from the epoch of the BH seed formation, we consider a system (BH and its host galaxy) to evolve in 'isolation' until a minor or major galaxy merger takes place.

Downloaded from https://academic.oup.com/mnras/article/476/1/407/4828380 by CNRS - ISTO user on 08 August 2022

the possibility of observationally distinguishing the two different populations of seed BHs.

The paper is organized as follows. In Section 2, we present the model for the SEDs. In Section 3, we discuss in detail two accreting heavy and two accreting light seed BH prototypes, inspecting their predicted SEDs. Finally, we discuss our results drawing the conclusions of the study in Sections 4 and 5.

2 SUMMARY OF THE MODEL

Here we summarize the main features of GAMETE/QSODUST, a semi-analytic, data-constrained model developed to study the formation and evolution of high-redshift quasars and their host galaxies in a cosmological framework. We refer the reader to Valiante et al. (2011, 2014, 2016, and Paper I, for further details on GAMETE/QSODUST).[2]

GAMETE/QSODUST successfully reproduced the observed properties of a sample of quasars at $z > 5$ (Valiante et al. 2014). Following V16, we focus our analysis on the progenitor BHs of the (2–6) $\times 10^9\,M_\odot$ SMBH that powers SDSS J1148+5251, one of the best studied luminous quasars at $z > 6$. A summary of the properties of SDSS J1148+5251 inferred from the observations can be found in Valiante et al. (2011, 2014).

DM halo merger trees. Different hierarchical merger histories (merger trees) of the $10^{13}\,M_\odot$ host DM halo have been reconstructed by using a Monte Carlo algorithm following the extended Press–Schechter theory. The DM halo resolution mass at $z > 14$ is extended to haloes with virial temperature in the range 1200 K $\leq T_{\rm vir} < 10^4$ K (i.e. mini-haloes). These mini-haloes dominate the halo mass spectrum at $z \gtrsim 17$ and are expected to host the first generation of stars (Pop III stars). At $z > 14$ instead, the merger tree halo population is dominated by Lyα haloes, namely DM haloes with $T_{\rm vir} \geq 10^4$ K (see V16 for details).

BH growth. The growth of the BH is driven by gas accretion and mergers. The BHAR is described by the Bondi–Hoyle–Lyttleton formula re-scaled by a factor $\alpha_{\rm BH} = 50$ (to match the BH mass of SDSS J1148+5251)[3] and cannot exceed the Eddington limit (see Valiante et al. 2014, for details).

Star formation and ISM chemical evolution. In each progenitor galaxy, stars are assumed to form following a series of quiescent and/or major merger-enhanced bursts.[4] Following each star formation episode, the production of metals and dust by asymptotic giant branch stars and supernovae (SNe) is regulated by the stellar lifetimes. In addition, we include physical prescriptions for dust processing in a two-phase ISM: destruction by SN shocks in the hot, diffuse medium and grain growth in cold, dense molecular clouds (see de Bennassuti et al. 2014; Valiante et al. 2014, for details).

Mechanical feedback. We also include energy-driven winds, triggered by SNe and accreting BHs. The metal and dust-rich gas outflows, launched on galaxy scales, are responsible for polluting the IGM. This mechanical feedback is described assuming that 0.2˜(0.25) per cent of the energy released by SN explosions (BH accretion) is used to accelerate the ISM gas (see Valiante et al. 2012, and V16 for details). As observed in SDSS J1148+5251 (Maiolino et al. 2012; Cicone et al. 2015), in our model the evolution history of BHs and their host galaxies is mainly regulated by AGN feedback, with SN-driven winds having only a minor effect.

2.1 First stars and BH seed formation

As discussed in V16, the number and nature of stars and BH seeds are determined by the combined effect of chemical and radiative feedback.

The level of chemical enrichment determines the duration of the Pop III star formation era. Pop III stars form out of metal-poor gas when the ISM metallicity is lower than the adopted critical threshold $Z_{\rm cr} \sim 10^{-4}\,Z_\odot$ (Schneider et al. 2002, 2003, 2012). The Pop III initial mass function (IMF) is assumed to be a Larson IMF (Larson 1998) with a characteristic mass $m_{\rm ch} = 20\,M_\odot$ (top-heavy IMF), whereas for Pop II we adopt $m_{\rm ch} = 0.35\,M_\odot$ (standard IMF).

In addition, the level of intensity of H_2 photodissociating radiation, to which haloes are exposed, determines whether stars (in mini-haloes) or DCBHs (in Lyα cooling haloes) form and regulates the star formation efficiency in mini-haloes (according to the halo virial temperature, redshift, and metallicity, see appendix A in V16 and de Bennassuti et al. 2017).

When the star formation efficiency is low, we perform a stochastic sampling of the intrinsic Pop III top-heavy IMF, randomly selecting stars in the mass range [10–300] $M_\odot$ until the total stellar mass formed in the burst is reached. Light BH seeds are formed by the collapse of Pop III stars with masses in the range [40–140] and [260–300] $M_\odot$.[5]

In Lyα cooling haloes, heavy BH seeds ($10^5\,M_\odot$) can form when $Z < Z_{\rm cr}$, and the cumulative Lyman–Werner (LW) emission (from all galaxies and AGN) is larger than the assumed critical value $J_{\rm cr} = 300 \times 10^{-21}$ erg s^{-1} Hz^{-1} cm^{-2} sr^{-1} (see Valiante et al. 2017, and references therein, for a discussion regarding $J_{\rm crit}$). As shown in V16, the critical level is reached at $z \sim 16$–18, depending on the particular merger history.

We stop forming Pop III stars and BH seeds at $z < 15$, when metal enrichment to $Z > Z_{\rm cr}$ triggers the transition to Pop II star formation.

3 SED MODELS

In this section, we describe how we derive the SED of galaxies hosting the first seed BHs. Once GAMETE/QSODUST has predicted the physical quantities for each galaxy and its central BH (i.e. the time-dependent BH mass, BHAR, gas density, star formation rate, stellar mass, ISM metallicity, and dust-to-gas ratio), we compute the expected intrinsic emission of the central accreting BH and stellar component, separately. Then, we process the combined emission by means of the plasma photoionization code CLOUDY, which models the physical conditions of clouds (ionization, chemical, and thermal state) exposed to emitting sources. Calculations were performed with version 13.04 of CLOUDY[6] (Ferland et al. 2013).

[2] The model GAMETE (GAlaxy MErger Tree and Evolution) was originally conceived to study the formation and evolution of local, Milky Way-like galaxies, in a cosmological context (Salvadori, Schneider & Ferrara 2007; Salvadori, Ferrara & Schneider 2008).

[3] $\alpha_{\rm BH}$ is a free parameter required in semi-analytic models and numerical simulations to account for the higher central densities around accreting BHs (e.g. Di Matteo, Springel & Hernquist 2005).

[4] A major merger is defined as the coalescence of two DM haloes with mass ratio (less massive over the most massive) $\mu > 1/4$.

[5] We assume that only the most massive BH among the Pop III remnants formed in each burst settles in the centre of the halo accreting gas from its surroundings.

[6] www.nublado.org

Downloaded from https://academic.oup.com/mnras/article/476/1/407/4828380 by CNRS - ISTO user on 08 August 2022

3.1 Stellar component

The intrinsic emission from Pop III stars is computed as the sum of single stellar black body (BB) spectra, depending on the randomly extracted stellar masses. We compute the BB by using the stellar effective temperatures given by Schaerer (2002).

The SEDs of Pop II stars are computed with the spectral evolution code PEGASE v2.0[7] (Fioc & Rocca-Volmerange 1997, 1999). As an input to the code, we provide the Larson IMF (not included in the original version) and the file containing the star formation and metallicity evolution histories (as a function of time, for each progenitor galaxy) as predicted by GAMETE/QSODUST.

3.2 Accreting BHs

The intrinsic SED of accreting BHs has been modelled as described in Pezzulli et al. (2017). The optical/UV primary emission from the accretion disc is the sum of multicolour BB spectra given by

$$L_\nu^{\rm BB} \propto \int_0^{T_{\rm max}} B_\nu(T) \left(\frac{T}{T_{\rm max}}\right)^{-11/3} \frac{{\rm d}T}{T_{\rm max}}, \quad (1)$$

where $B_\nu(T)$ is the Planck function and T the disc temperature, which reaches the maximum value, $T_{\rm max}$, nearby the innermost stable circular orbit. $T(r)$ is the temperature profile of steady-state, optically thick, geometrically thin accretion disc described by Shakura & Sunyaev (1973, see Pezzulli et al. 2017 for further details). The template spectrum is normalized to the accreting BH bolometric luminosity.

The part of the spectrum in the X-ray energy band due to the emission from the hot corona is modelled with a power law with an exponential cut-off at energy $E_{\rm c} = 300$ keV (Sazonov, Ostriker & Sunyaev 2004; Yue et al. 2013): $L_\nu \propto \nu^{-\Gamma+1} {\rm e}^{-h\nu/E_{\rm c}}$. We include the contribution of the metallicity-dependent reflection component (the primary X-ray emission reflected by the surrounding neutral medium) using the reflection-only solution of the PEXRAV model (Magdziarz & Zdziarski 1995) in the XSPEC code.[8]

Following Brightman et al. (2013), we consistently compute the photon index, Γ, in the hard X-ray band (2–10 keV) for each accreting BH as a function of the Eddington ratio $\lambda_{\rm Edd}$ (predicted by GAMETE/QSODUST) as $\Gamma_{2-10\,{\rm keV}} = 0.32 \log \lambda_{\rm Edd} + 2.27$.

3.3 Emerging spectrum

The AGN and stellar intrinsic emission components are used as an input to CLOUDY. The emerging SED is the result of the total intrinsic radiation reprocessed by the column of gas, enriched by atomic metals and dust, present in the host galaxy.

We assume a static, spherical geometry for the material distribution within the galaxy. In CLOUDY, the spherical gas cloud configuration is described by distributing the material in concentric shells with progressively larger radii. The inner shell face is illuminated by the radiation coming from a combination of point-like sources placed at the centre.

To compute the emerging spectrum, CLOUDY requires the following set of parameters:

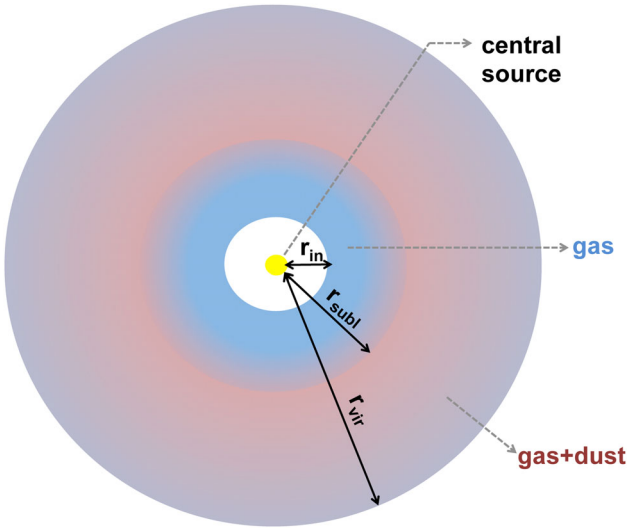

Figure 1. Schematic view of the geometry adopted for CLOUDY simulations (see the text for details). Different black solid arrows show the inner, $r_{\rm in}$, sublimation, $r_{\rm subl}$, and DM halo virial radius, $r_{\rm vir}$. Dust-free gas is distributed in the inner $r < r_{\rm subl}$ shell, while the dusty ISM of the host extends from $r_{\rm subl}$ to $r_{\rm vir}$.

(i) inner and outer radii of the sphere, $r_{\rm in}$ and $r_{\rm out}$;

(ii) gas number density at the inner radius $n(r_{\rm in})$ and the power index, α, of the gas radial density profile;

(iii) gas composition: column of hydrogen, helium, atomic metals (or gas metallicity), and dust-to-gas ratio.

In GAMETE/QSODUST, the gas density profile is described by a singular isothermal sphere with a flat core:

$$n(r) = \frac{n_{\rm norm}}{1 + (r/r_{\rm core})^2}. \quad (2)$$

The term $n_{\rm norm}$ is the normalization constant set by the condition that the total gas mass of the galaxy is enclosed within the halo virial radius, $R_{\rm vir}$. A core radius of $r_{\rm core} = 0.1\,(0.01)$ pc has been chosen to encompass the small scale of the inner, higher density regions around the central accreting heavy (light) seed BH.[9]

We adopt the inner radius $r_{\rm in} = r_{\rm core}$ and the number density $n(r_{\rm in}) = n_{\rm norm}$ as input values for the CLOUDY simulations and select the CLOUDY density profile $n(r) = n(r_{\rm in})(r/r_{\rm in})^\alpha$ cm^{-3}, with $\alpha = 2$, that closely match the profile of equation (2) adopted in the GAMETE/QSODUST calculation. The outer radius is set to be $r_{\rm out} = R_{\rm vir}$. A schematic representation of the adopted geometry is given in Fig. 1.

The host galaxy metallicity and dust-to-gas ratio predicted by GAMETE/QSODUST are transferred to the CLOUDY computation by re-scaling the built-in table 'ISM' abundances, which accounts for metals and dust mixtures.[10]

We have verified that dust grains in the very inner regions (i.e. in the shells closer to the emitting source) can be heated above the sublimation limit. In other words, the maximum temperature

[7] http://www2.iap.fr/users/fioc/PEGASE.html

[8] We consistently linked Γ, $E_{\rm c}$, and normalization parameter to the values adopted for the primary power-law component and set the inclination angle to 60° and the reflection strength parameter, $R = 1$, consistent with typical values of local low-luminosity AGN (Burlon et al. 2011; Del Moro et al. 2017; Zappacosta et al. 2018).

[9] As a comparison, the radius of gravitational influence of a BH, $\sim G M_{\rm BH}/c_{\rm s}^2$, is ~3 pc for $M_{\rm BH} = 10^5$ M$_\odot$ ($c_{\rm s} \sim 15$ km s^{-1} for $T_{\rm gas} = 10^4$ K) and ~0.03 pc for $M_{\rm BH} = 100$ M$_\odot$ ($c_{\rm s} \sim 5$ km s^{-1} for $T_{\rm gas} = 10^3$ K).

[10] In CLOUDY, the 'ISM' gas-phase abundances are from Cowie & Songaila (1986), Savage & Sembach (1996), Snow, Destree & Jensen (2007), and Mullman et al. (1998), and the dust grain model is from Mathis, Rumpl & Nordsieck (1977).

Downloaded from https://academic.oup.com/mnras/article/476/1/407/4828380 by CNRS - ISTO user on 08 August 2022

of a grain species exceeds the default sublimation temperature (1400 and 1750 K for silicate and graphite grains, respectively). Ignoring this aspect may overestimate the IR emission. To account for dust sublimation, when required, we perform simulations with CLOUDY adopting the following three-step strategy (runs).

(i) We determine the dust sublimation radius, $r_{\rm subl}$ (with $r_{\rm subl} > r_{\rm in}$), at which the temperature of the hottest grain species first falls below the sublimation temperature (run 1).

(ii) We process the accreting BH emission travelling through the inner dust-free shell of depth $r_{\rm subl} - r_{\rm in}$. Thus, the inner shell of the cloud is heated only by the AGN (run 2).

(iii) We combine the transmitted BH emission, resulting from run 2, with the emission from stellar sources and give the resulting SED as an input for a third CLOUDY simulation for the outer shells, $r_{\rm subl} \leq r \leq r_{\rm out}$ (run 3).

This three-step simulation strategy allows us to approximately mimic the fact that the AGN and stellar emission do not come from the same location in the host galaxy and are expected to be reprocessed by different gas and dust column densities. It is reasonable to assume that star-forming regions are located on scales of few hundreds of pc (e.g. Davies et al. 2006, 2007; Hicks et al. 2009; Wada, Papadopoulos & Spaans 2009; Sani et al. 2012) where dusty molecular clouds can survive the destructive effects of the strong radiation field of the central AGN (i.e. in overdense regions where the cold, molecular gas is shielded by dust).

Finally, we include the redshift-dependent cosmic microwave background radiation field, modelled by CLOUDY as a BB spectrum with temperature $T_{\rm CMB} = T_0(1+z)$ K (Peebles 1971; Wilkinson 1987; Mather et al. 1999).

4 RESULTS

In this section, we compute the time-dependent SED of four prototypical ILS and IHS along their evolution. Since our main aim is to investigate if the nature of BH seeds can be observationally discriminated, we select two efficiently growing and two inefficiently growing BH seeds among the IHS and ILS samples. In this way, we highlight differences in the same population of systems and similarities among the two different classes. In what follows, we indicate each system by its host halo ID assigned in the simulation merger tree.

4.1 Most and least massive BH in the sample

We have selected the most and least massive BH, in the sample analysed in Paper I. The physical and observational properties of these systems are representative of sources that we expect to find in biased regions that lead to the formation of a SMBH at $z > 6$.

Fig. 2 shows the evolution of selected ILS and IHS systems in the BH–stellar mass plane. The differences among the four tracks are indicative of the large variety of evolutionary channels that we find in the simulation.

The two IHS (2538 and 13356) are shown by the solid and dashed lines. Initially, they follow a similar evolution at constant BH mass. When the stellar mass of the hosts has reached a value of 10^3 M$_\odot$, the BH mass of 2538 grows faster than the stellar mass, reaching a value of $\sim 10^7$ M$_\odot$, whereas 13356 continues to evolve at an almost constant BH mass. It is interesting to compare the evolution of these two systems with the average evolution of IHS, shown by the pink circles. It shows that 2538 better represents the average evolution of IHS hosted in galaxies with $M_{\rm star} \leq 10^{4.5}$ M$_\odot$. The

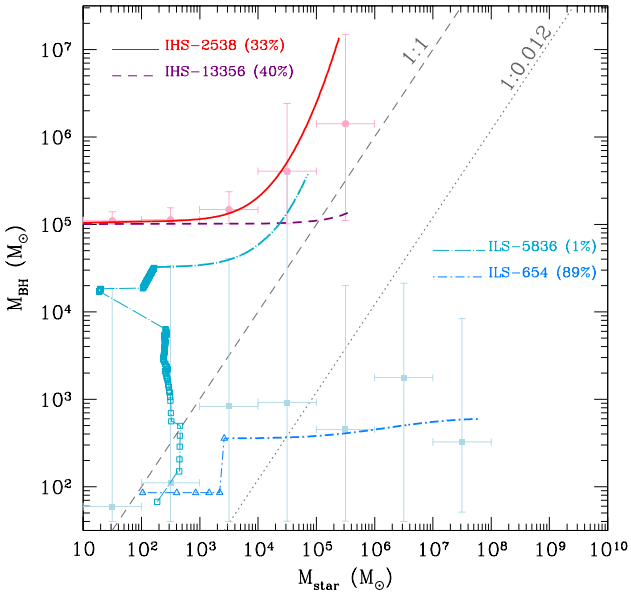

Figure 2. The BH mass as a function of the stellar mass for the selected accreting seed BH prototypes. Solid and dashed lines are IHS-2538 and 13356, respectively. Two ILS are instead shown with dot–dashed (654) and dot–long dashed (5836) curves. For these systems, data points indicated by squares (triangles) indicate the evolution during the Pop III star formation regime. We also label the fraction of systems in the IHS and ILS populations showing properties similar to each prototype (see the text for details). Filled light blue squares and pink circles represent, respectively, the average BH mass of ILS and IHS in different stellar mass bins, with bars indicating the maximum and minimum BH mass in each bin and the width of the stellar mass interval. The dotted and short-dashed lines indicate the 1:1 and local BH–stellar mass (Sani et al. 2011) scaling relations.

fraction of systems similar to IHS-2538 ($\sim$33 per cent) and 13356 ($\sim$40 per cent) are also labelled in the figure. The remaining fraction of objects instead shows mixed properties in terms of final BH mass and/or lifetime in isolation (Δt, see fig. 2 in Paper I).

The two ILS (5836 and 654) are shown by dot–dashed and dot–long dashed lines, respectively. Triangle-shaped (squared) data points indicate their growth during the Pop III star formation epoch (see Appendix for further details). They start with comparable BH mass but follow a very different evolution. ILS-5836 grows much faster than the stellar mass (squares) until Pop II stars start to form in the host halo (dot–long dashed line) whereas ILS-654 evolves at an almost constant BH mass. In both systems, the central BHs experience mergers with other Pop III BHs formed in the same host galaxies (see section 3.2 in Paper I). These events cause the step-like increase in the BH mass along the two tracks (see Appendix). The comparison with the average evolution of ILS, shown by the light blue squares, indicates that ILS-654 is more representative of the average ILS evolution. About 89 per cent of systems are similar to ILS-654 while systems following an evolution (in terms of BH mass) similar to ILS-5836 are only $\sim$1 per cent of the population,[11] as labelled in the figure.

A detailed description of evolutionary histories of the four prototypical systems is given in Appendix.

We define the age of each system as the time it spends evolving in isolation from the formation of the BH seed (age = 0). The

[11] Here we are considering all systems with $M_{\rm BH} > 2 \times 10^4$ M$_\odot$ for this estimate.

Downloaded from https://academic.oup.com/mnras/article/476/1/407/4828380 by CNRS - ISTO user on 08 August 2022

isolated evolution ends when the first (minor or major) halo merger occurs. It is worth mentioning that although we follow systems in the 'isolated' phase, this does not imply that the selected host haloes evolve in isolation prior to seed BH formation. Thus, the initial conditions (e.g. gas mass and metallicity at age = 0) are different in different systems, even in those belonging to the same class. This reflects the different histories prior to BH seed formation and the host halo selection: ILS are initially hosted in star-forming mini-haloes, while IHS hosts are Lyα cooling haloes.

The four selected systems account for the large diversity in the properties of ILS and IHS populations. By looking at individual evolutionary histories (see Fig. A1), we infer that BH growth is affected by (i) the environmental conditions at the epoch of BH seed formation (i.e. the properties of the host halo resulting from its earlier evolution) and, afterwards, (ii) by the host galaxy star formation and chemical enrichment histories. The final BH mass, at the end of the isolated evolution, is largely determined by these properties. Systems with similar (ILS-5836 and 654) or even equal (IHS-2538 and 13356) initial seed mass can follow very different evolutionary tracks reaching final BH masses that differ by ∼2 orders of magnitude. Systems hosting BHs of different origins (IHS-2538 and ILS-5836) may instead end up having similar properties (during certain stages of their evolution). These differences/similarities are reflected in the predicted SEDs.

4.2 Emission from BH seeds and their hosts

Following the procedure described in Section 3, we compute the SED of the selected IHS and ILS presented above at different times of their evolution (ages). Clearly, these correspond to different redshifts in the simulation. The results are shown in Fig. 3. The SEDs are represented by lighter colours at wavelengths where the emission will be completely absorbed by the intervening neutral hydrogen along the line of sight. These correspond to rest-frame wavelengths shortwards of the Lyman limit at 912 Å, down to about ∼100 Å (Madau 1995; Inoue et al. 2014, and references therein). In each panel, the yellow shaded and cyan dashed regions indicate the observed hard, [2–10] keV, and soft, [0.5–2] keV, X-ray bands. The grey arrow in the X-ray part of the spectrum identifies the range in the limiting fluxes of the *ATHENA* survey designed by Aird et al. (2013) for a ∼1 deg^2 (lower end) and ∼100 deg^2 (upper end) area.[12] The grey triangles and squares report the NIRcam and MIRI photometric sensitivities onboard of *JWST*.[13]

4.2.1 *The most massive systems*

We first analyse the time-dependent spectra of IHS-2538 (top left) and ILS-5836 (bottom left), which have been selected to be the most massive BHs among the IHS and ILS samples (see Fig. 2). At each epoch, the spectrum of IHS-2538 is dominated by the AGN continuum emission, resulting in an almost featureless SED (no prominent, luminous emission lines can be identified). Although strongly attenuated by the intervening material, the most prominent feature in the rest-frame SED is the optical/UV emission from the BH accretion disc (the big blue bump). The reprocessed AGN emission extends to $\lambda_{\rm obs} \sim 10\,\mu$m.[14] At longer wavelengths, the SED is dominated by dust thermal emission. At age ≥ 100 Myr, when the BH mass is $M_{\rm BH} > 7 \times 10^5\,{\rm M}_\odot$ and the BHAR is $\dot{M}_{\rm BH} > 0.01\,{\rm M}_\odot\,{\rm yr}^{-1}$ (see the top-left panel in Fig. A1), the rest-frame optical–UV emission is redshifted to the near-IR (NIR) bands and is detectable by NIRcam. At almost the same time, the emission in the X-ray bands becomes intense enough to exceed the lower flux limit in the *ATHENA* survey.

The duration of the isolated evolution of ILS-5836 is comparable to that of IHS-2538 (∼225 Myr), but this system is located at a much higher redshift. It forms at $z \sim 22.9$ and evolves in isolation down to $z \sim 12$. At age = 0, when the first Pop III stars form, the emission from the accreting ∼100 M$_\odot$ BH is comparable to that coming from the stellar component. As the system evolves in time, the emission properties appear to be a scaled-down version of IHS-2538 (see also the bottom-left panel of Fig. A1). However, more prominent emission lines are present. This is a consequence of the larger gas column density in the host galaxy of ILS-5836, due to the less efficient BH feedback. At age = 250 Myr, although its flux is still below the *JWST* limit, the SED of ILS-5836 is potentially indistinguishable, in terms of shape and spectral features, from that of IHS-2538.

4.2.2 *The least massive systems*

Quite different spectra are predicted for IHS-13356 and ILS-654, which have been selected to host the two inefficiently growing BHs among the IHS and ILS sample (see Fig. 2). The SEDs of IHS-13356 are shown in the top-right panel of Fig. 3 at age = 0, 5, and 16 Myr. At age = 0, the only emitting source is the newly planted BH. Its radiation travels through a large gas column density, as the gas mass is ∼20 times higher than in IHS-2538 at the same epoch (as discussed in the previous section). Among the several emission lines, H and He recombination lines are present. Although the continuum level is below the NIRcam photometric capability, some of the lines are intense enough to be detected by NIRspec, despite the very high redshift of the source. As the gas mass drops, at age ≥ 5 Myr, the spectra are dominated by the continuum. At 16 Myr, the part of the spectrum (magenta dot–dashed line) entering in the NIRcam filters at $1\,\mu{\rm m} < \lambda_{\rm obs} < 3\,\mu$m is dominated by the stellar component ($M_* \sim 10^5\,{\rm M}_\odot$) and it is just above the sensitivity limits. At this stage, IHS-13356 emission could be revealed by NIRcam (*F*200*W* and *F*277*W* filters) onboard of *JWST*. This low-mass, inefficiently accreting BH is predicted to be too faint to be detected in the X-ray bands, even with *ATHENA* sensitivity.

Finally, the bottom-right panel of Fig. 3 shows the SED of the starburst-dominated ILS-654. Similarly to IHS-13356, this is a slowly accreting light BH seed whose mass never exceeds ∼10^3 M$_\odot$, even after 400 Myr of evolution. The continuum emission is dominated by the stellar component with the low-mass AGN contributing to the X-ray part of the spectrum, but the emission remains several orders of magnitude fainter than any current (and

[12] This survey has been designed as a Wide Field Imager wedding cake strategy with single tiers of 4 × 1Ms, 20 × 300 ks, 75 × 100 ks, and 259 × 30 ks. Reported flux limits are for a 3 arcsec point spread function. A collecting area of $2m^2$ at 1 keV and an instrument field of view of 40 arcmin × 40 arcmin have been assumed.

[13] These are the photometric performance requirements of the instruments, namely the point source faintest fluxes that can be obtained at a signal-to-noise ratio SNR = 10 in a 10 ks integration (https://jwst.stsci.edu/science-planning/proposal-planning-toolbox/sensitivity-overview).

[14] We do not include polycyclic aromatic hydrocarbon particles in the computation, which are expected to radiate in the [1−−13] μm range.

Downloaded from https://academic.oup.com/mnras/article/476/1/407/4828380 by CNRS - ISTO user on 08 August 2022

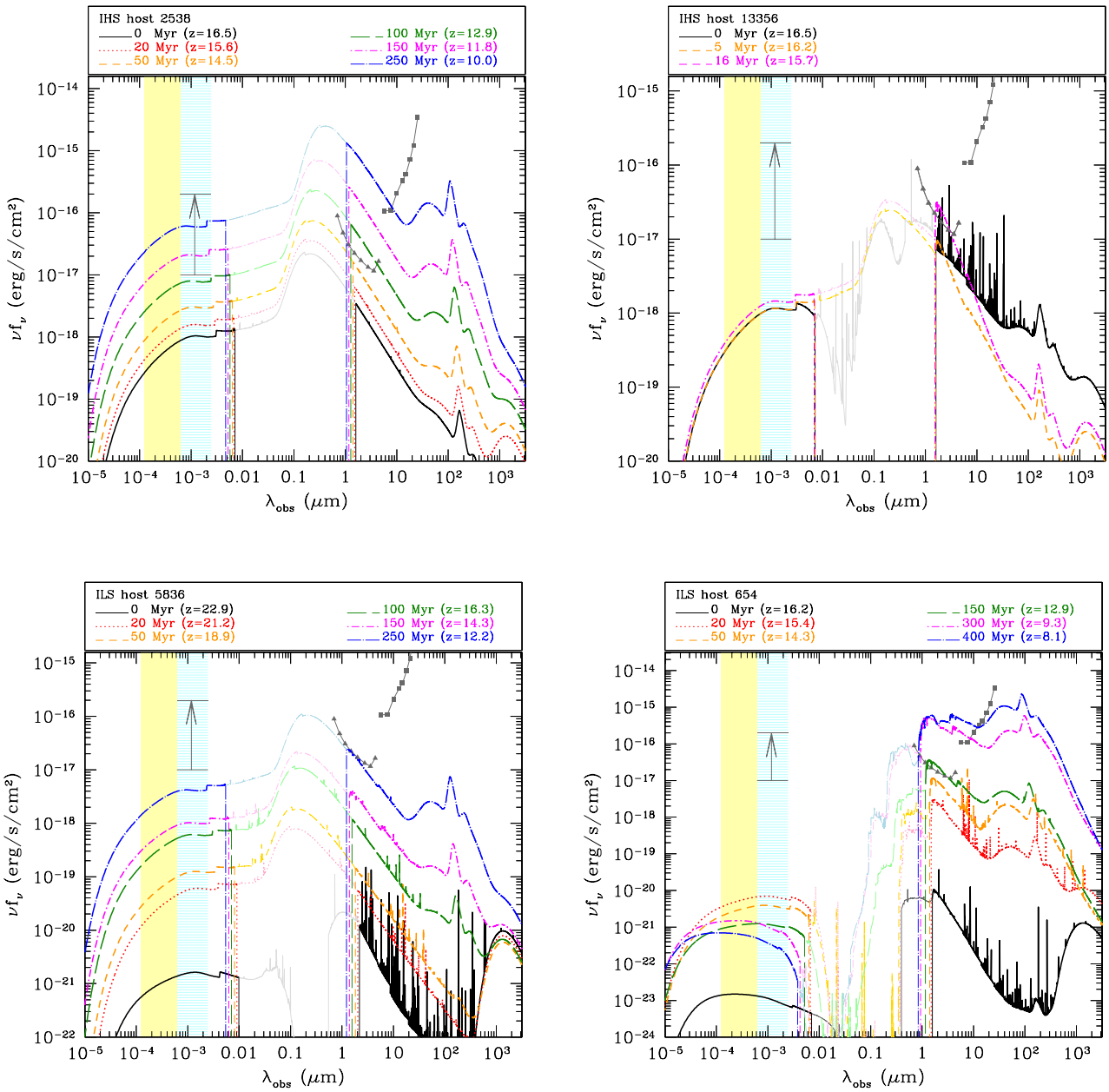

Figure 3. SED of IHS-2538 (top left), IHS-13356 (top right), ILS-5836 (bottom left), and ILS-654 (bottom right) as a function of the observed wavelength, $\lambda_{\rm obs}$. In each panel, different lines correspond to different ages of the system, as shown by the legends, where we also label the corresponding redshift in the simulation. The SEDs are shown by lighter colours at wavelengths where the emission will be completely absorbed by the intervening neutral hydrogen along the line of sight. The yellow shaded and cyan dashed regions indicate the observed hard and soft X-ray bands, respectively. The vertical arrow marks the flux limit of future surveys designed for the *ATHENA* mission by Aird et al. (2013). The grey triangles and squares are the photometric flux limits of the instruments NIRcam and MIRI on the *JWST*.

future) instrument sensitivity. As the galaxy evolves (age > 100 Myr), a continuum-dominated spectrum emerges. Such an intense stellar emission may be easily revealed by the *JWST*.

4.2.3 Detectability

To summarize, systems like IHS-2538 or ILS-654 in the latest stages of their evolution (age $\gtrsim$ 100 Myr) could be easily detected by the *JWST* instruments NIRcam (at $\lambda \geq 0.9\,\mu$m) and MIRI (at least in the two higher sensitivity photometric filters, *F*560*W* and *F*770*W*). The NIR and mid-IR (MIR) luminosities of these objects are $L_{\rm NIR} \gtrsim 10^{42}\,{\rm erg\,s^{-1}}$ and $L_{\rm MIR} \gtrsim 10^{43}\,{\rm erg\,s^{-1}}$, respectively.[15] On the other hand, detecting objects like ILS-5836 would instead require deeper NIRcam campaigns. Interestingly, we find that the emission from a pure accreting heavy seed (no stars) enshrouded in a dense gas cloud, as in IHS-13356, may be revealed already at $z > 16$ by the spectrograph NIRspec, thanks to its prominent emission lines. The stellar-dominated radiation emerging afterwards (at $z \sim 15.7$)

[15] These are the NIR and MIR band luminosities provided by CLOUDY in the wavelength ranges [1–5] and [5−−40] μm, respectively.

Downloaded from https://academic.oup.com/mnras/article/476/1/407/4828380 by CNRS - ISTO user on 08 August 2022

may be instead detected in the *F*200*W* and *F*227*W* NIRcam filters. Finally, the *ATHENA* survey programme envisioned in Aird et al. (2013) will reach flux limits that are exceeded only by accreting BH seeds similar to IHS-2538 at age > 100 Myr, when their soft X-ray luminosity becomes $L_{[0.5-2]\,\mathrm{keV}} \geq 10^{42}\,\mathrm{erg\,s^{-1}}$.

We conclude that light and heavy seeds and their hosts can have very different emission properties. However, these appear to be more significantly affected by their individual evolutionary history rather than by their initial nature, i.e. whether they classify as a light or heavy BH seed. Yet, we recall that the two 'antithetical' seed prototypes, IHS-2538 and ILS-654, show very different emission spectra: the first one being dominated by the central AGN and the second one being dominated by the stellar component of the host galaxy. While ILS-654 better represents the average evolution of light seeds, IHS-2538 represents ∼33 per cent of the IHS population. Still, systems like IHS-2538 are the most luminous among the IHS, thus, having the largest probability of being detected by *JWST*.

4.3 The mean IHS

As discussed above, the four selected prototypes represent extreme cases (the most and least efficiently growing IHS and ILS). In the ILS population, the results obtained for ILS-654 are also representative of the average population (see Fig. 2). Thus, in order to make our predictions for IHS systems more general, we perform an additional analysis, by investigating the SEDs and observational properties of the 'average' IHS population. To this aim, we have constructed and processed AGN and stellar emission obtained by considering the average IHS evolution shown in Fig. 2 (pink data points). The evolution of the mean IHS host has been weighted over the average lifetime in isolation, ∼65 Myr (obtained from the distribution discussed in Paper I).[16]

The mean IHS is an AGN-dominated system and its evolution is very similar (in both normalization and spectral features) to IHS-2538, although its final BH is less massive (∼1.4 × $10^6\,\mathrm{M_\odot}$ at 65 Myr). For this reason, we do not show the predicted time-dependent SED. In particular, in the final stage of the mean IHS (i.e. at age = 65 Myr), its SED is comparable to that of IHS-2538 at age = 100 Myr (with the mean IHS being potentially detectable by *JWST*). This is consistent with the fact that at these stages, when the BH mass is $\lesssim 10^6\,\mathrm{M_\odot}$, IHS-2538 and the mean IHS grow following similar evolutionary tracks.

4.4 Observational features of BH seeds and their hosts

To investigate the observability of growing BH seeds, we consider the systems presented above, and compute their colours in the NIRcam filters and their X-ray luminosities.

To this aim, we first take the SED of each system during its brightest phase, which corresponds to different ages and redshifts (see Fig. 3). Bolometric luminosities of systems at the brightest stage are given in Table 1. During these phases, all the systems reach AB magnitudes $M_{\mathrm{AB}} < 29$, above the *JWST* sensitivity limit for a 10 ks exposure in the [0.7−4.4] μm spectral band.[17]

Then, we shift the above SED at $z = 9$, 10, 11, 13, and 15, in order to compare the four systems at the same redshift.[18] This approach enables us to provide more general predictions, independently of the redshift at which the brightest stage is reached.

To compare with previous studies, we adopt the same colour–colour diagram proposed by Natarajan et al. (2017). The resulting $F090W - F200W$ versus $F200W - F444W$ colour–colour diagram is shown in Fig. 4. The predicted colours reflect different galaxy types, with AGN-dominated systems (such as IHS-2538 and ILS-5836) being bluer than starbursts (ILS-654). The two classes are clearly distinguishable in the colour–colour plane, independently of their redshifts. Despite its lower AB magnitude,[19] we predict

Table 1. Bolometric luminosities of systems during the brightest stage of their evolution (see the text for details).

Name	Age (Myr)	Redshift	$L_{\mathrm{bol}}(\mathrm{erg\,s^{-1}})$
IHS-2538	250	∼10	$\sim 10^{45}$
IHS-13356	16	∼16	$\sim 4 \times 10^{43}$
mean IHS	65	∼13.9	$\sim 9.2 \times 10^{43}$
ILS-5836	225	∼12	$\sim 5 \times 10^{43}$
ILS-654	405	∼8.1	$\sim 3.5 \times 10^{44}$

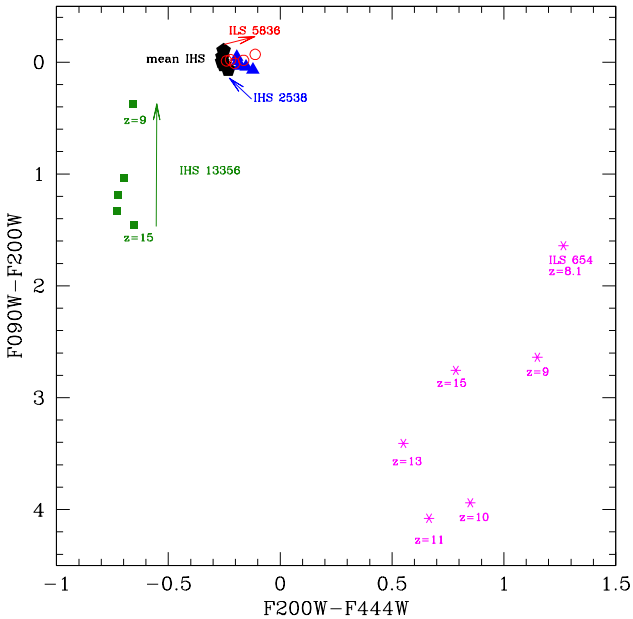

Figure 4. The colour–colour diagram for the selected prototypes at $z = 9$, 10, 11, 13, and 15. IHS like 2538 and 13356 are shown by triangles and squares, respectively. Black pentagons are for the mean IHS case. ILS like 5836 and 654 are shown by circles and asterisks, respectively. For ILS-654, we also show the case $z = 8.1$, corresponding to the redshift at which the host reaches its maximum luminosity, at age = 400 Myr (see the text). For other sources, the arrows indicate the decreasing redshift direction.

[16] For the mean IHS, age=0 corresponds to the average formation redshift of heavy seeds, that is $z \sim 16.5$, the same redshift at which IHS-2538 forms. The final redshift, after ∼65 Myr of isolated evolution, corresponds to $z \sim 13.9$.

[17] The four selected systems are *F*090*W* dropouts, as the Lyman limit (912 Å) is redshifted to longer wavelengths, with the exception of ILS-654 at age ≥ 300 Myr (i.e. at $z \leq 9$).

[18] At $z \geq 10$, these must be considered as upper limits as the Lyman limit (912 Å rest frame) falls in the *F*090*W* filter at these redshifts.

[19] ILS-5836 reaches $M_{\mathrm{AB}} \sim 29$ only at the end of its isolated evolution, at $z \sim 12$, and would be detectable with NIRcam at lower redshifts.

Downloaded from https://academic.oup.com/mnras/article/476/1/407/4828380 by CNRS - ISTO user on 08 August 2022

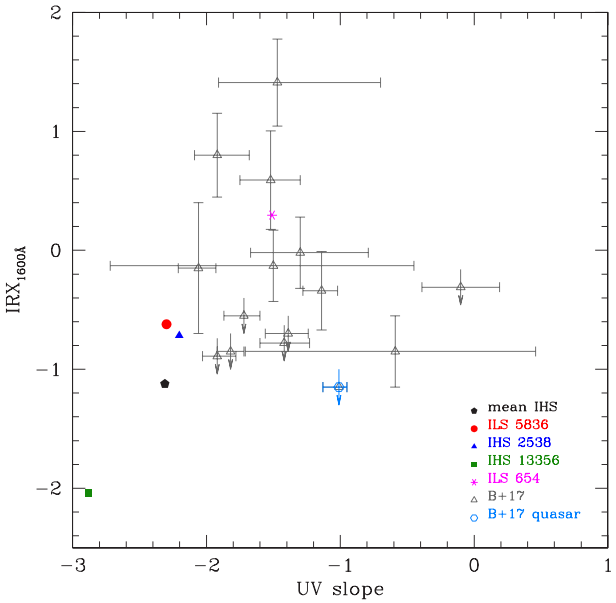

Figure 5. The IRX as a function of the UV continuum slope. Filled symbols represent IHS (2538 – blue triangle, 13356 – green square, mean IHS – black pentagon) and ILS hosts (5836 – red circle, 654 – magenta asterisk). Open data points with error bars are from Barisic et al. (2017), with the hexagon indicating a quasar candidate at $z = 5.3$.

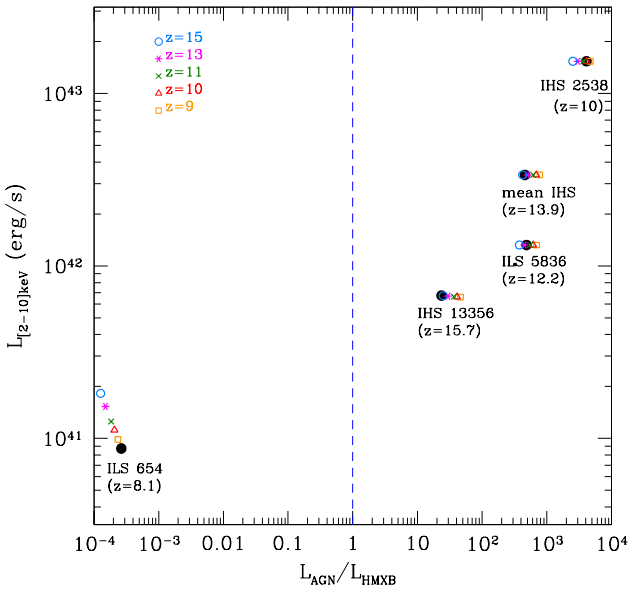

Figure 6. The relative contribution of accreting BHs and HMXBs to the luminosity at [2−10] keV for the four prototypes in our sample: IHS-2538, IHS-13356, ILS-5836, and ILS-654, and the mean IHS. Black filled circles show the luminosity at the original redshift of the system while open coloured symbols indicate the predictions at $z = 9$ (yellow squares), 10 (red triangles), 11 (green crosses), 13 (magenta asterisks), and 15 (azure circles). The blue vertical line depicts an equal contribution from AGN and HMXBs.

ILS-5836 to have very similar colours to IHS-2538. Hence, independently of their nature and of their redshifts, we find that efficiently growing BH seeds occupy a well-defined region of the colour–colour diagram.

In Fig. 5, we show the IR excess (IRX)–UV slope diagram for the same systems and compare the results with the sample of $z \sim 5.5$ galaxies presented by Barisic et al. (2017). We compute the ratio between the rest-frame IR and UV luminosities as IRX = log ($L_{\rm IR}/L_{1600\,\text{Å}}$) and the UV continuum slopes, β, as a least-squares linear fit in the [1500–3000] Å part of the spectra. Since the IRX is related to dust extinction, it is not surprising that the dustiest ($D_{\rm ISM} \sim 5 \times 10^{-4}$, see Fig. A1) starburst prototype ILS-654 shows a high IRX, 0.29, and a spectral slope $\beta = -1.51$, consistent with some of the $z \sim 5.5$ observed galaxies (Mancini et al. 2016; Barisic et al. 2017). The IR luminosity (integrated from 8 to 1000 μm) of this system is $L_{\rm IR} \sim 10^{44}$ erg s^{-1} (∼85 per cent of the bolometric luminosity).

As expected, based on the similarity of their SED and colours, IHS-2538 and ILS-5836 have similar IRX and UV slopes. In these systems, the UV light from the accreting BHs is only mildly absorbed by the poorly enriched ISM of their host galaxies (see Fig. A1), resulting in a lower IRX, ∼0.6–0.7, than in ILS-654. The mean IHS show a lower IRX with respect to IHS-2538 as a consequence of the lower associated dust-to-gas ratio (estimated by averaging over the dust-to-gas ratio of all the IHS systems). With respect to ILS-5836, the IRX of mean IHS is lower because of its higher $L_{1600\,\text{Å}}$.

Finally, the exceptionally blue slope ($\beta \sim -2.88$) and low IRX (~ -2.04) of IHS-13356 reflect the almost unattenuated, pure stellar emission dominating the SED at its maximum. The predicted β slope is consistent with the mean colour of faint $z \sim 7$ galaxies measured by Bouwens et al. (2010).

The properties discussed above can be used to identify accreting BH seed candidates in future *JWST* surveys, distinguishing them from starbursts.

By combining the information obtained from colour–colour and IRX–β diagrams, we suggest that the best candidates for future and deeper X-ray follow-up observational campaigns should be selected according to the following conditions:

(i) $-0.3 \lesssim F200W - F444W \lesssim 0$ and $F090W - F200W \gtrsim -0.2$
(ii) UV continuum slopes $\beta < -2$ and $-1.5 < \text{IRX} < 0$.

One additional limitation to the observational identification of growing BH seeds is that the X-ray luminosities of faint BHs are hard to discriminate from the cumulative emission of high-mass X-ray binaries (HMXBs) in the host galaxies (e.g. Volonteri et al. 2017). In Fig. 6, we show the hard X-ray band luminosity, $L_{[2-10]\,\text{keV}} = L_{\rm AGN} + L_{\rm HMXB}$, as a function of the ratio between the AGN and HMXB luminosities, $L_{\rm AGN}/L_{\rm HMXB}$, in the same spectral band. Following Volonteri et al. (2017), $L_{\rm HMXB}$ is computed using the empirical relation found by Lehmer et al. (2016), $\log(L_{\rm HMXB}) = 39.82 + 0.63\log\dot{M}_* + 1.31\log(1+z)$, at the original redshift of the system in the simulation and at redshifts $z = 9$, 10, 11, 13, and 15.[20]

We find that systems with properties similar to IHS-2538, the mean IHS, and ILS-5836 have $L_{\rm AGN}/L_{\rm HMXB} > 100$. These would be easily identified as AGN. Although the SED of IHS-13356 is dominated by stellar emission (see Fig. 3) in the optical/UV (rest-frame) part of the spectrum, a star formation rate of $\dot{M}_* \sim 0.027\,\text{M}_\odot\,\text{yr}^{-1}$ (see Fig. A1) corresponds to a population of HMXBs that produce less than ∼5 per cent of the total luminosity at [2–10] keV ($L_{\rm AGN} \sim 6.5 \times 10^{41}$ erg s^{-1} while $L_{\rm HMXB} \sim 2.7 \times 10^{40}$ erg s^{-1}). On the other hand, the hard X-ray luminosity of IHS-654 would be dominated by HMXBs.

[20] The contribution of HMXBs has been computed only for the purpose of this comparison, and it is not included in the SED models presented in Fig. 3.

Downloaded from https://academic.oup.com/mnras/article/476/1/407/4828380 by CNRS - ISTO user on 08 August 2022

Our analysis shows that systems hosting rapidly growing BH seeds at their centre (such as IHS-2538 and ILS-5836) can be easily discriminated from systems where the BH is almost inactive and/or the dominant emission comes from the host galaxy (such as ILS-654 and IHS-13356). They show bluer colours, intermediate IRX values, and a high luminosity in the hard X-ray band, largely dominated by the accreting BH. On the other hand, the discrimination of the nature of the BH seed, whether it formed as a Pop III stellar remnant or as a DCBH, can be done only on the basis of statistical arguments.

5 COMPARISON WITH PREVIOUS WORKS

In their recent works, Pacucci et al. (2015) and Natarajan et al. (2017) suggest that *JWST* will also be able to discriminate among DCBH and Pop III remnant seeds by means of their spectral features. Similarly, we have explored the SED of growing DCBHs and Pop III remnant BHs, comparing the expected spectral features of the two different channels, in the same spirit of these earlier works but with some important differences.

The post-processing with CLOUDY that we perform in our study is complementary to the one adopted by Natarajan et al. (2017). They consider an idealized set-up of a halo at a given redshift (with a given metallicity) while in our model the galaxy properties (e.g. the metallicity and dust-to-gas ratio) are derived from the cosmological evolution of the haloes.

The adopted initial gas density profile in the model of Pacucci et al. (2015) results in SED with more prominent emission lines (mainly H and He recombination lines). In our simulation, similar gas densities and IR spectral features are found in haloes 13356 and 5836, in the very early stages of their evolution, at ages $< 5-20$ Myr, when – however – AGN are faint $L_{\rm bol} \leq 10^{43}$–10^{42}, respectively.

On the other hand, the systems investigated by Natarajan et al. (2017) are the peculiar, transient OBGs (Agarwal et al. 2013). These are different from our IHS and ILS hosts, from the evolutionary point of view. In the scenario predicted by Agarwal et al. (2013), the newly formed DCBH hosts merge with a nearby star-forming galaxy soon after the formation of the seed, in less than $\sim$1 Myr. We find that, in a comparable time-scale, star formation in IHS hosts is enabled by the fast metal enrichment driven by gas-rich inflows from the IGM. Systems similar to IHS-2538, the most massive accreting heavy seed, at the end of their isolated evolution have properties consistent with an OBG, in terms of stellar and BH mass.[21]

If compared with previous works, our model shows how the emission depends on the environmental conditions in which the BH seeds form and grow. These conditions are determined by the assembly history of the $z \sim 6$ SMBH and its host galaxy.[22] Our predictions are for sources that would be seen in biased (overdense) regions where $z > 6$ SMBHs form and, thus, are somehow complementary with respect to other works.

In overdense regions, the evolution of massive seeds (DCBHs) may be faster (more efficient) than in average volumes of the Universe (unbiased regions). In the latter case, the ISM evolution is strongly dominated by star formation, where SN feedback regulates the growth (and the feedback strength) of BH seeds in low-mass galaxies at early cosmic epochs (e.g. Dubois et al. 2015; Anglés-Alcázar et al. 2017; Bower et al. 2017; Habouzit, Volonteri & Dubois 2017; Trebitsch et al. 2017). In this scenario, growing BH seeds are similar to IHS-13356.

Conversely, in biased regions where $z > 6$ SMBHs are expected to form, the early growth of some massive BH seeds ($\sim$33 per cent of the IHS population in our model) is self-regulated by AGN feedback, as star formation (and thus SN feedback) is quenched as a consequence of the rapid build-up of an intense UV background radiation (see appendix A in Paper I and V16 for details). The comparison with other studies, thus, points to a different evolution in biased (overdense) and unbiased (average volumes) regions. This is consistent with the discussion presented in Paper I.

In deep blank-field surveys, we expect that sources predicted in our model would be seen in overdense regions that will later form $z \sim 6$ quasars (i.e. protoclusters; e.g. Overzier 2016).

We find that a colour–colour selection, similar to that proposed by Natarajan et al. (2017), would help in distinguishing AGN-dominated galaxies from starbursts. Although they have similar AB magnitudes ($M_{\rm AB} \leq 26$ in the NIRcam bands), ILS-654-like starbursts are expected to be redder than OBGs and IHS-2538-like systems. On the other hand, despite the lower AB magnitude rapidly growing ILS-5836-like systems have colours similar to IHS-2538-like ones, comparable to those expected for $z \sim 11$ OBGs. Thus, we find that a colour–colour selection is capable of uniquely identifying the nature of BH seeds only in a statistical sense. In fact, as we will show in the next section, rapidly growing BH seeds that originate from DCBHs have a higher probability of being detected, in agreement with previous findings (Pacucci et al. 2015; Natarajan et al. 2017).

Another source of confusion in tracing the observational features of the first accreting BHs has been recently pointed out by Volonteri et al. (2017). The authors show that in high-redshift galaxies, hosting $<$1 Gyr old stellar populations may be very difficult to distinguish stellar and AGN emission at rest-frame UV/optical wavelengths. Moreover, the emission from low-mass AGN (powered by 10^5–10^6 $M_\odot$ BHs) and from HMXB at [2–10] keV would be difficult to disentangle at $z > 6$. The observational strategy we have suggested above would help in overcoming such a confusion problem.

6 SUMMARY AND CONCLUSIONS

In Paper I, we have investigated the physical properties of galaxies hosting light and heavy seeds in a cosmological context, following the formation and evolution of the first stars and BHs along the hierarchical assembly of a $z = 6.4$ quasar like SDSS J1148+5251. In this work, we have used those properties to model the SEDs of both accreting BHs and their stellar counterparts, taking into account their redshift/time evolution as well as the effect of the interplay between, chemical, mechanical, and radiative feedback on the host galaxies.

To this aim, we have selected four interesting objects from our sample of accreting BHs, two of which representative of the high-mass end of their population distributions, and two in the low-mass end, to emphasize differences and similarities between the two classes. We have extracted their evolutionary properties as long as their host galaxies evolve in isolation, only through mass exchanges

[21] For example, after living in isolation for 250 Myr, at $z = 10$, the IHS-2538 host galaxy merges with a normal star-forming galaxy (not hosting a BH in its centre) with a stellar mass of $\sim 3 \times 10^7$ $M_\odot$ (before the merger). The properties of the galaxy formed by this merger are very similar to those expected for the OBGs discussed by Agarwal et al. (2013): the BH mass is $\sim 2 \times 10^7$ $M_\odot$ and the stellar mass is $\sim 4 \times 10^7$ $M_\odot$.

[22] The assembly history determines the interplay between different physical processes (e.g. Pop III/Pop II star formation, onset of DCBH seeding conditions, BH growth, build-up of UV background, etc.) and their effects on the environment (via chemical, mechanical, and radiative feedback).

Downloaded from https://academic.oup.com/mnras/article/476/1/407/4828380 by CNRS - ISTO user on 08 August 2022

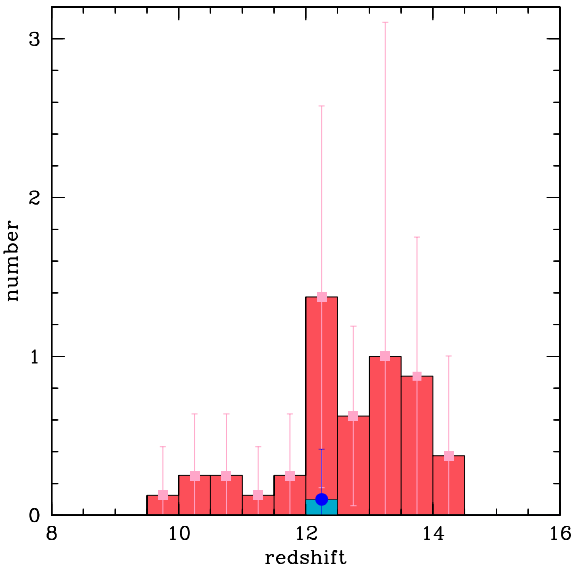

Figure 7. The redshift distribution of detectable IHS (red) and ILS (blue). Histograms and data points show the average number over 10 different realizations with error bars indicating the 1σ dispersion. In each redshift bin, we show the number of systems with $L_{\rm bol} \geq 4 \times 10^{43}$ erg s^{-1} ($M_{\rm BH} \geq 3.5 \times 10^5$ M$_\odot$).

with the external medium (infall/outflows), with no mergers. Still, the evolution of these objects is influenced by (and influence) the evolution of the other galaxies polluting the external medium with metals and dust and permeating the virtual volume in which they reside with photodissociating and ionizing radiation.

For the selected objects, we modelled the intrinsic emission coming from the accreting BHs and the stars. We then used these templates to predict the SED emerging from the host galaxy by processing the intrinsic emission using the software CLOUDY. The information required to compute both the intrinsic and reprocessed emission, namely the Pop III remnant BH mass, BHAR, and the properties of their host galaxies, such as the time-evolving gas density, metallicity, and dust-to-gas ratio, was all consistently computed by the model GAMETE/QSODUST.

Our study attempts to answer two important questions: (i) Can we detect the (growing) BH seed progenitors of the first SMBHs? and if yes, (ii) Can we identify the nature of BH seeds?

To answer the first question, we confirm that future, high-sensitivity facilities and missions, like *JWST* and *ATHENA*, will be able to detect the most luminous ($L_{\rm NIR} \geq 10^{42}$ erg s^{-1}; $L_{\rm MIR} \geq 10^{43}$ erg s^{-1}; $L_{[0.5-2]\,\rm keV} \geq 10^{42}$ erg s^{-1}) progenitors of the first SMBHs.

Regarding the second question, searches for growing BH seeds must be extended out to $z > 10$, when the probability of observing them in isolation is expected to be higher (see Paper I). It is also interesting to note that at $z \lesssim 15(17)$, for IHS (ILS), at least half of the BHs are still in isolated systems. At lower redshift, BH seeds and their host galaxies rapidly lose memory of their initial conditions (see Paper I for details).

Among $z > 6$ SMBH progenitors, rapidly growing BH seeds at $z > 10$ that are luminous enough to be detectable with *JWST*, in the field of a quasar, are only 2 per cent of the total BH seed population. This percentage corresponds to an average number of $\sim 4^{+3}_{-2}$ (at a 1σ confidence level, assuming Poissonian statistics) progenitors for each $z \sim 6$ SMBH. Their average redshift distribution is shown in Fig. 7, where we also discriminate IHS (red histogram) and ILS (blue histogram). Hence, a *JWST* detected BH progenitor at $z > 10$ has a larger probability to originate from a DCBH than from a Pop III remnant. Our conclusion is that it will be difficult to discriminate the nature of $z \sim 6$ SMBH seeds on the basis of their observational features as Pop III BHs and DCBHs look very similar when they are above *JWST* or *ATHENA* sensitivity limits. However, if detected, these systems are more likely powered by a growing DCBH.

Interestingly, with a 10 ks NIRcam observation, sources like IHS-13356 can be detected with a SNR =10 in the *F*200*W* and *F*277*W* filters, already at $z \sim 15.7$. In addition, we foresee that blind search programmes conducted with the spectrograph NIRspec would allow us to reveal these kinds of systems even at earlier epochs ($z > 16$), thanks to the strong emission lines emerging in the spectra.

We believe that a multi-wavelength approach will be fundamental in searching the first SMBH progenitors. While *JWST* will be able to characterize their host galaxies, the high *ATHENA* flux sensitivity ($\sim 10^{-17}$ erg s^{-1} cm^{-2} at [0.5–2] keV; Nandra et al. 2013) will allow us to uncover the signatures of accreting BHs. A IR colour–colour plus IRX–β selection of high-redshift *JWST* sources could help in successfully identifying possible SMBH progenitor candidates in future X-ray surveys, also providing a unique tool for preparing follow-up observations.

Finally, we stress that the above conclusions apply to a scenario where SMBHs at $z \sim 6$ originate from the Eddington-limited growth of Pop III BHs and DCBHs. If Pop III stellar remnants are able to sustain short and intermittent phases of super-Eddington accretion (Pezzulli et al. 2016), their occurrence and observational properties may be different.

ACKNOWLEDGEMENTS

The research leading to these results has received funding from the European Research Council under the European Union's Seventh Framework Programme (FP/2007-2013)/ERC Grant Agreement no. 306476. LZ acknowledges financial support under ASI/INAF contract 1/037/12/0. We thank Angela Bongiorno, Fabrizio Fiore, Emanuele Giallongo, Michele Ginolfi, Andrea Grazian, Tilman Hartwig, Elisabeta Lusso, and Laura Pentericci for fruitful discussions.

REFERENCES

Agarwal B., Davis A. J., Khochfar S., Natarajan P., Dunlop J. S., 2013, MNRAS, 432, 3438
Agarwal B., Dalla Vecchia C., Johnson J. L., Khochfar S., Paardekooper J.-P., 2014, MNRAS, 443, 648
Agarwal B., Johnson J. L., Zackrisson E., Labbe I., van den Bosch F. C., Natarajan P., Khochfar S., 2016, MNRAS, 460, 4003
Agarwal B., Johnson J. L., Khochfar S., Pellegrini E., Rydberg C.-E., Klessen R. S., Oesch P., 2017, MNRAS, 469, 231
Aird J. et al., 2013, preprint (arXiv:1306.2325)
Anglés-Alcázar D., Faucher-Giguère C.-A., Quataert E., Hopkins P. F., Feldmann R., Torrey P., Wetzel A., Kereš D., 2017, MNRAS, 472, L109
Barisic I. et al., 2017, ApJ, 845, 41
Begelman M. C., Volonteri M., Rees M. J., 2006, MNRAS, 370, 289
Bouwens R. J. et al., 2010, ApJ, 708, L69
Bower R. G., Schaye J., Frenk C. S., Theuns T., Schaller M., Crain R. A., McAlpine S., 2017, MNRAS, 465, 32
Bowler R. A. A., McLure R. J., Dunlop J. S., McLeod D. J., Stanway E. R., Eldridge J. J., Jarvis M. J., 2017, MNRAS, 469, 448
Brightman M. et al., 2013, MNRAS, 433, 2485
Bromm V., Loeb A., 2003, ApJ, 596, 34
Burlon D., Ajello M., Greiner J., Comastri A., Merloni A., Gehrels N., 2011, ApJ, 728, 58

Downloaded from https://academic.oup.com/mnras/article/476/1/407/4828380 by CNRS - ISTO user on 08 August 2022

Cappelluti N. et al., 2016, ApJ, 823, 95
Chon S., Hirano S., Hosokawa T., Yoshida N., 2016, ApJ, 832, 134
Cicone C. et al., 2015, A&A, 574, A14
Cowie L. L., Songaila A., 1986, ARA&A, 24, 499
Davies R. I. et al., 2006, ApJ, 646, 754
Davies R. I., Müller Sánchez F., Genzel R., Tacconi L. J., Hicks E. K. S., Friedrich S., Sternberg A., 2007, ApJ, 671, 1388
de Bennassuti M., Schneider R., Valiante R., Salvadori S., 2014, MNRAS, 445, 3039
de Bennassuti M., Salvadori S., Schneider R., Valiante R., Omukai K., 2017, MNRAS, 465, 926
Del Moro A. et al., 2017, ApJ, 849, 57
Di Matteo T., Springel V., Hernquist L., 2005, Nature, 433, 604
Dijkstra M., Ferrara A., Mesinger A., 2014, MNRAS, 442, 2036
Dijkstra M., Gronke M., Sobral D., 2016, ApJ, 823, 74
Dubois Y., Volonteri M., Silk J., Devriendt J., Slyz A., Teyssier R., 2015, MNRAS, 452, 1502
Ferland G. J. et al., 2013, Rev. Mex. Astron. Astrofis., 49, 137
Ferrara A., Salvadori S., Yue B., Schleicher D., 2014, MNRAS, 443, 2410
Fioc M., Rocca-Volmerange B., 1997, A&A, 326, 950
Fioc M., Rocca-Volmerange B., 1999, preprint (arXiv:e-prints)
Gallerani S., Fan X., Maiolino R., Pacucci F., 2017, PASA, 34, e022
Georgakakis A. et al., 2015, MNRAS, 453, 1946
Giallongo E. et al., 2015, A&A, 578, A83
Habouzit M. et al., 2016, MNRAS, 456, 1901
Habouzit M., Volonteri M., Dubois Y., 2017, MNRAS, 468, 3935
Haiman Z., 2004, ApJ, 613, 36
Hartwig T., Glover S. C. O., Klessen R. S., Latif M. A., Volonteri M., 2015, MNRAS, 452, 1233
Heger A., Fryer C. L., Woosley S. E., Langer N., Hartmann D. H., 2003, ApJ, 591, 288
Hicks E. K. S., Davies R. I., Malkan M. A., Genzel R., Tacconi L. J., Müller Sánchez F., Sternberg A., 2009, ApJ, 696, 448
Hirano S., Hosokawa T., Yoshida N., Omukai K., Yorke H. W., 2015, MNRAS, 448, 568
Hosokawa T., Omukai K., Yorke H. W., 2012, ApJ, 756, 93
Hosokawa T., Yorke H. W., Inayoshi K., Omukai K., Yoshida N., 2013, ApJ, 778, 178
Inayoshi K., Haiman Z., 2014, MNRAS, 445, 1549
Inayoshi K., Omukai K., 2012, MNRAS, 422, 2539
Inayoshi K., Omukai K., Tasker E., 2014, MNRAS, 445, L109
Inayoshi K., Visbal E., Kashiyama K., 2015, MNRAS, 453, 1692
Inoue A. K., Shimizu I., Iwata I., Tanaka M., 2014, MNRAS, 442, 1805
Johnson J. L., Haardt F., 2016, PASA, 33, e007
Larson R. B., 1998, MNRAS, 301, 569
Latif M. A., Ferrara A., 2016, PASA, 33, e051
Latif M. A., Schleicher D. R. G., Schmidt W., Niemeyer J. C., 2013, MNRAS, 436, 2989
Lehmer B. D. et al., 2016, ApJ, 825, 7
Lodato G., Natarajan P., 2006, MNRAS, 371, 1813
Lodato G., Natarajan P., 2007, MNRAS, 377, L64
Luo B. et al., 2017, ApJS, 228, 2
Madau P., 1995, ApJ, 441, 18
Madau P., Rees M. J., 2001, ApJ, 551, L27
Madau P., Rees M. J., Volonteri M., Haardt F., Oh S. P., 2004, ApJ, 604, 484
Magdziarz P., Zdziarski A. A., 1995, MNRAS, 273, 837
Maiolino R. et al., 2012, MNRAS, 425, L66
Mancini M., Schneider R., Graziani L., Valiante R., Dayal P., Maio U., Ciardi B., 2016, MNRAS, 462, 3130
Mather J. C., Fixsen D. J., Shafer R. A., Mosier C., Wilkinson D. T., 1999, ApJ, 512, 511
Mathis J. S., Rumpl W., Nordsieck K. H., 1977, ApJ, 217, 425
Matthee J., Sobral D., Santos S., Röttgering H., Darvish B., Mobasher B., 2015, MNRAS, 451, 400
Mullman K. L., Lawler J. E., Zsargó J., Federman S. R., 1998, ApJ, 500, 1064
Nandra K. et al., 2013, preprint (arXiv:1306.2307)
Natarajan P., 2011, preprint (arXiv:1105.4902)
Natarajan P., Pacucci F., Ferrara A., Agarwal B., Ricarte A., Zackrisson E., Cappelluti N., 2017, ApJ, 838, 117
Overzier R. A., 2016, A&AR, 24, 14
Pacucci F., Ferrara A., Volonteri M., Dubus G., 2015, MNRAS, 454, 3771
Pacucci F., Ferrara A., Grazian A., Fiore F., Giallongo E., Puccetti S., 2016, MNRAS, 459, 1432
Pacucci F., Pallottini A., Ferrara A., Gallerani S., 2017, MNRAS, 468, L77
Pallottini A. et al., 2015, MNRAS, 453, 2465
Peebles P. J. E., 1971, Physical Cosmology. Princeton Univ. Press, Princeton, NJ
Petri A., Ferrara A., Salvaterra R., 2012, MNRAS, 422, 1690
Pezzulli E., Valiante R., Schneider R., 2016, MNRAS, 458, 3047
Pezzulli E., Valiante R., Orofino M. C., Schneider R., Gallerani S., Sbarrato T., 2017, MNRAS, 466, 2131
Reines A. E., Comastri A., 2016, PASA, 33, e054
Salvadori S., Schneider R., Ferrara A., 2007, MNRAS, 381, 647
Salvadori S., Ferrara A., Schneider R., 2008, MNRAS, 386, 348
Sani E., Marconi A., Hunt L. K., Risaliti G., 2011, MNRAS, 413, 1479
Sani E. et al., 2012, MNRAS, 424, 1963
Savage B. D., Sembach K. R., 1996, ARA&A, 34, 279
Sazonov S. Y., Ostriker J. P., Sunyaev R. A., 2004, MNRAS, 347, 144
Schaerer D., 2002, A&A, 382, 28
Schneider R., Ferrara A., Natarajan P., Omukai K., 2002, ApJ, 571, 30
Schneider R., Ferrara A., Salvaterra R., Omukai K., Bromm V., 2003, Nature, 422, 869
Schneider R., Omukai K., Bianchi S., Valiante R., 2012, MNRAS, 419, 1566
Shakura N. I., Sunyaev R. A., 1973, A&A, 24, 337
Smidt J., Wiggins B. K., Johnson J. L., 2016, ApJ, 829, L6
Smith A., Bromm V., Loeb A., 2016, MNRAS, 460, 3143
Snow T. P., Destree J. D., Jensen A. G., 2007, ApJ, 655, 285
Sobral D., Matthee J., Darvish B., Schaerer D., Mobasher B., Röttgering H. J. A., Santos S., Hemmati S., 2015, ApJ, 808, 139
Sugimura K., Coppola C. M., Omukai K., Galli D., Palla F., 2016, MNRAS, 456, 270
Tanaka T., Haiman Z., 2009, ApJ, 696, 1798
Trebitsch M., Volonteri M., Dubois Y., Madau P., 2017, preprint (arXiv:1712.05804)
Treister E., Schawinski K., Volonteri M., Natarajan P., 2013, ApJ, 778, 130
Valiante R., Schneider R., Salvadori S., Bianchi S., 2011, MNRAS, 416, 1916
Valiante R., Schneider R., Maiolino R., Salvadori S., Bianchi S., 2012, MNRAS, 427, L60
Valiante R., Schneider R., Salvadori S., Gallerani S., 2014, MNRAS, 444, 2442
Valiante R., Schneider R., Volonteri M., Omukai K., 2016, MNRAS, 462, 3146 (V16)
Valiante R., Agarwal B., Habouzit M., Pezzulli E., 2017, PASA, 34, e031
Valiante R., Schneider R., Graziani L., Zappacosta L., 2018, MNRAS, 474, 3825 (Paper I)
Visbal E., Haiman Z., Bryan G. L., 2016, MNRAS, 460, L59
Vito F. et al., 2016, MNRAS, 463, 348
Volonteri M., 2010, A&AR, 18, 279
Volonteri M., Rees M. J., 2005, ApJ, 633, 624
Volonteri M., Rees M. J., 2006, ApJ, 650, 669
Volonteri M., Haardt F., Madau P., 2003, ApJ, 582, 559
Volonteri M., Lodato G., Natarajan P., 2008, MNRAS, 383, 1079
Volonteri M., Silk J., Dubus G., 2015, ApJ, 804, 148
Volonteri M., Reines A., Atek H., Stark D. P., Trebitsch M., 2017, ApJ, 849, 155
Wada K., Papadopoulos P. P., Spaans M., 2009, ApJ, 702, 63
Weigel A. K., Schawinski K., Treister E., Urry C. M., Koss M., Trakhtenbrot B., 2015, MNRAS, 448, 3167
Wilkinson D. T., 1987, in Ulmer M. P., ed., 13th Texas Symposium on Relativistic Astrophysics. World Scientific Press, Singapore, p. 209
Willott C. J., 2011, ApJ, 742, L8
Yoshida N., Omukai K., Hernquist L., 2008, Science, 321, 669
Yue B., Ferrara A., Salvaterra R., Xu Y., Chen X., 2013, MNRAS, 433, 1556

Downloaded from https://academic.oup.com/mnras/article/476/1/407/4828380 by CNRS - ISTO user on 08 August 2022

Yue B., Ferrara A., Salvaterra R., Xu Y., Chen X., 2014, MNRAS, 440, 1263
Zappacosta L. et al., 2018, ApJ, 854, 33

APPENDIX: PROPERTIES OF INDIVIDUAL SYSTEMS

In this appendix, we provide a detailed description of the evolutionary histories of the four prototypical systems.

We present the time-dependent properties of systems IHS-2538, IHS-13356, ILS-5836, and ILS-654 in Fig. A1. For each system, in the upper panel, we show the DM (dotted line), gas (dashed), stellar (dot–dashed), and BH (solid) masses. In the upper horizontal axis, we also label the redshifts in the simulation that correspond to the different ages. The star formation rate and BHAR are shown in the middle panel with dot–dashed and solid lines, respectively. Finally, the lower panel reports the gas-phase metals ($Z_{\rm ISM}$, dot–dashed line) and dust-to-gas mass ratio ($D_{\rm ISM}$, dashed line) in the ISM (in absolute units). For comparison, we also show the critical metallicity, $Z_{\rm cr} \sim 10^{-4}\,{\rm Z}_\odot$ (dotted horizontal line), which marks the transition from Pop III to Pop II star formation.

IHS-2538: This is one of the most massive and longest-living IHS. By construction, the initial BH has a mass of $10^5\,{\rm M}_\odot$ and forms in a Lyα cooling halo ($M_{\rm h} \sim 5 \times 10^7\,{\rm M}_\odot$) at redshift $z = 16.5$. Such a DM halo is the descendant of two sterile mini-haloes. For its entire history, the heavy seed grows close to or at the Eddington rate. Efficient BH feeding and feedback enable the galaxy to sustain only a very low star formation rate ($<3 \times 10^{-3}\,{\rm M}_\odot\,{\rm yr}^{-1}$). As a result, the BH always grows faster than the stellar component, and the SED properties are expected to be dominated by the AGN emission.

IHS-13356: This is one of the shortest-living and smallest IHS. Differences in the histories of IHS-13356 progenitors, relative to IHS-2538, lead to different initial gas masses at age = 0. The reason for this behaviour can be understood as follows: newly virialized haloes gradually accrete their gas mass following an exponentially decaying infall rate until they merge with another halo (i.e. they do not instantaneously acquire the universal baryon fraction $\Omega_{\rm b}/\Omega_{\rm M}$; see equation 3 and further details in Salvadori et al. 2008). IHS-13356 is hosted in a Lyα cooling halo formed by the merger of two sterile mini-haloes at $z = 16.5$. These ancestors virialize at $z \sim 17$ and accrete a gas mass that corresponds to ~40 per cent of $\Omega_{\rm b}/\Omega_{\rm M}$ prior to their coalescence. Conversely, IHS-2538 is hosted in a Lyα cooling halo that has formed soon after its progenitor mini-haloes virialize, so that they accrete only ~1 per cent of $\Omega_{\rm b}/\Omega_{\rm M}$ by the time they coalesce. When IHS-13356 forms, the coalescence of its gas-rich ancestors triggers an efficient starburst of $\sim 2 \times 10^{-2}\,{\rm M}_\odot\,{\rm yr}^{-1}$. The gas mass suddenly drops from $\sim 2 \times 10^6$ to $\sim 10^5\,{\rm M}_\odot$ within the first 0.5 Myr, corresponding to the time-step of the simulation at that redshift. Thereafter, IHS-13356 evolves in gas starvation, with star formation, BH accretion, and the associated mechanical feedback depleting almost all the gas mass that the halo is accreting from the IGM. At the end of the brief (16 Myr) isolated evolution, the nuclear BH mass has increased by ~50 per cent and the stellar mass is a factor of ~2.5 larger. The emission properties of this system are dominated by the AGN during the first 5 Myr of the evolution (when $M_* < 10^5\,{\rm M}_\odot$), and by the emission of the host galaxy thereafter.

ILS-5836: This is one of the most massive ILS. Its host halo is one of the first star-forming mini-haloes ($M_{\rm h} \sim 4 \times 10^6\,{\rm M}_\odot$) at redshift $z \sim 23$. Due to its pristine composition, a first burst of Pop III stars ($10^{-3}\,{\rm M}_\odot\,{\rm yr}^{-1}$) leads to the formation of one massive BH remnant with $M_{\rm BH} \sim 70\,{\rm M}_\odot$. Pop III star formation continues for about 100 Myr, down to redshift $z \sim 16.2$, but with a ~50 Myr suppression due to the effect of the LW flux at which the mini-halo is exposed. Due to their short evolutionary time-scales, massive Pop III stars are assumed to evolve in one simulation time-step (instantaneous recycling approximation). Hence, $M_* = 0$ when the $\dot{M}_* = 0$. When the DM halo has become a Lyα cooling halo, Pop III star formation turns on again and continues until metal enrichment triggers the transition to Pop II star formation, in the last ~125 Myr of evolution. During the Pop III regime, the nuclear BH grows by gas accretion and mergers with other remnant BHs forming in subsequent bursts, reaching a mass of $\sim 10^4\,{\rm M}_\odot$ in ~70 Myr. The gas accretion rate triggered during the non-star-forming phase leads to a BH dominance scenario even in the subsequent Pop II star formation regime: in ILS-5836, the BH mass continues to grow faster than its stellar counterpart. At $z \sim 12.2$, the BH mass has grown to $4 \times 10^5\,{\rm M}_\odot$. This evolution is reflected in the SED, which is a sort of scaled-down version of the SED of IHS-2538.

ILS-654: This is one of the least massive but longest-living ILS. Inefficient BH accretion [$\dot{M}_{\rm BH} \sim (10^{-7}{-}10^{-6})\,{\rm M}_\odot\,{\rm yr}^{-1}$] leads to a final mass of only $800\,{\rm M}_\odot$ in more than 400 Myr of evolution. Although they have similar initial BH masses and accretion rates, $\sim 10^{-6}\,{\rm M}_\odot\,{\rm yr}^{-1}$ at age = 0, BH growth in ILS-5836 at early times is mainly driven by mergers with other Pop III BH remnants during the prolonged Pop III star formation in this halo. As a consequence of the low BH growth of ILS-654, the available gas mass can efficiently fuel star formation, yielding to a star formation rate $>0.01\,{\rm M}_\odot\,{\rm yr}^{-1}$ already at age > 30 Myr. The evolution of ILS-654 is indeed consistent with that of a normal star-forming galaxy, and the system becomes the most metal-rich of the four selected objects. In addition, in the absence of efficient BH accretion and feedback, more infalling gas is retained and the higher metallicity, dust-to-gas ratio, and gas density are reflected in the predicted SED.

Downloaded from https://academic.oup.com/mnras/article/476/1/407/4828380 by CNRS - ISTO user on 08 August 2022

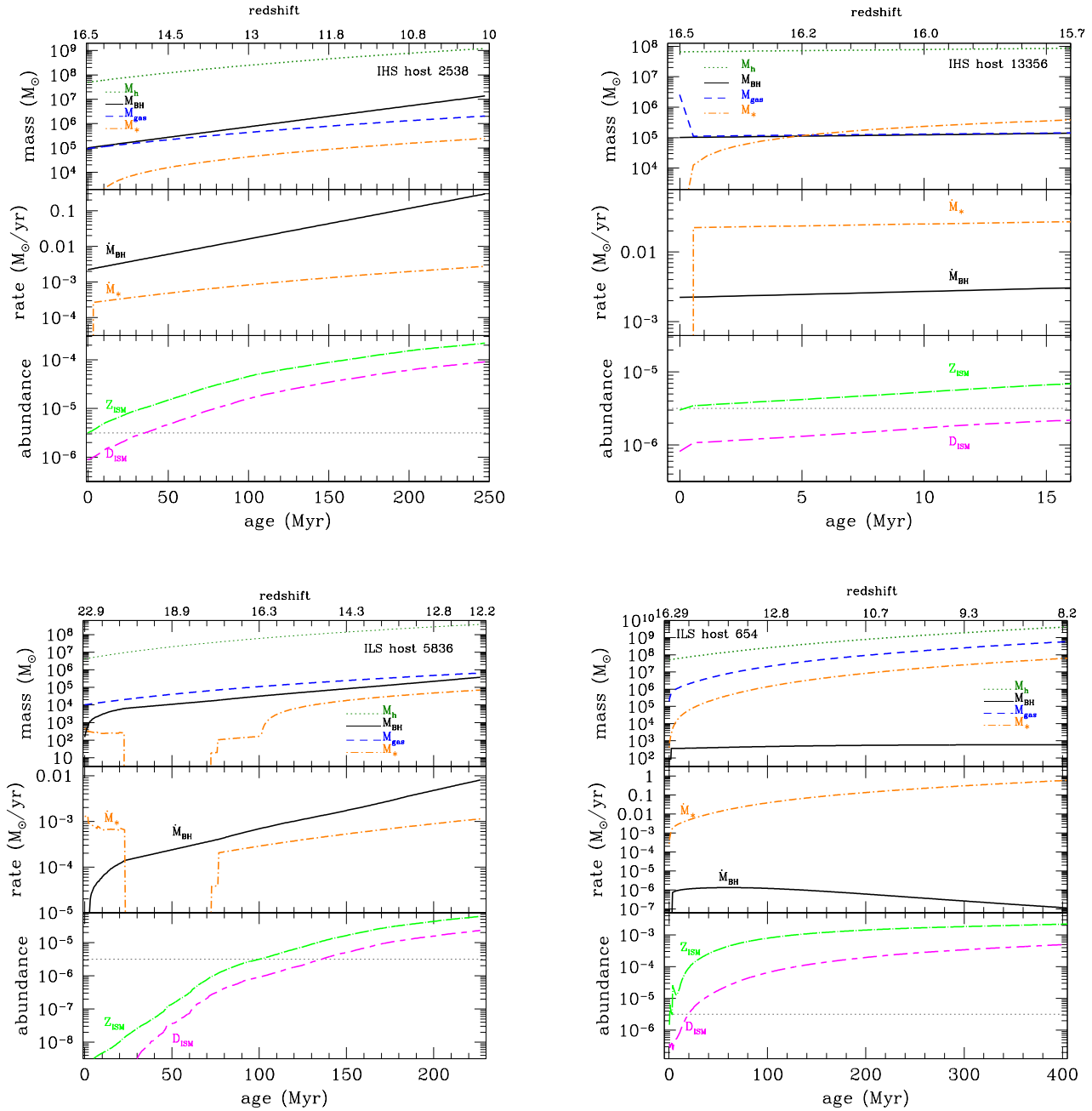

Figure A1. Time-dependent properties of IHS-2538 (top left), IHS-13356 (top right), ILS-5836 (bottom left), and ILS-654 (bottom right). For each system, the upper panel shows the DM halo (dotted line), gas (dashed line), stellar (dot–dashed line), and BH (solid line) masses. The middle panel shows the star formation (dot–dashed) and black hole accretion (solid) rates. The lower panel shows the metallicity (dot–dashed line) and dust-to-gas mass ratio (dashed line) of the ISM, in absolute units. The horizontal dotted line indicates the critical metallicity for the Pop III/Pop II star transition.

This paper has been typeset from a TEX/LATEX file prepared by the author.

Downloaded from https://academic.oup.com/mnras/article/476/1/407/4828380 by CNRS - ISTO user on 08 August 2022